

*Transactions, SMiRT-26*  
Berlin/Potsdam, Germany, July 10-15, 2022  
Division I

## **LARGE-SCALE CAST-IN-PLACE PRACTICE OF SPECIAL CONCRETE FOR NUCLEAR REACTOR BUILDINGS - ULTRA-HIGH- PERFORMANCE CONCRETE WITH A SPECIFIED COMPRESSIVE STRENGTH OF 150 MPA**

**Di Qiao<sup>1</sup>, Yukiko Nishioka<sup>1</sup>, Masaro Kojima<sup>1</sup>, Daisuke Honma<sup>1</sup>, Kazuyuki Torii<sup>2</sup>  
Gentaro Nagashima<sup>3</sup>, Kensuke Morita<sup>4</sup>, Ritsu Hagiwara<sup>5</sup>**

<sup>1</sup> Takenaka Corporation, Inzai, Chiba, Japan (qiao.di@takenaka.co.jp)

<sup>2</sup> Shimizu Corporation, Tokyo, Japan

<sup>3</sup> Mitsubishi Heavy Industries, Ltd., Hyogo, Japan

<sup>4</sup> Hitachi-GE Nuclear Energy, Ltd., Ibaraki, Japan

<sup>5</sup> Toshiba Energy Systems & Solutions Corporation, Kanagawa, Japan

### **ABSTRACT**

This study investigated the large-scale cast-in-place applicability of a designed ultra-high-performance concrete (UHPC) mixture reinforced with a hybrid of steel and polypropylene fibers containing coarse aggregates. It addressed several issues on application to nuclear reactor buildings, in particular the mass concrete. The properties of the UHPC, including working time, thermal and autogenous strains, strength development, steel fiber orientation, and rebar probe for installing post anchors, were experimentally studied. The test results showed that the UHPC mixture exhibited comparable casting performance with conventional concrete following Japan's existing building standards. Although the highest temperature at the specimen center was measured at 78 degrees Celsius, no thermal cracking was observed. All samples for testing compressive strength showed satisfactory results, and the compressive strength correlated well with the cumulative temperature-time following a logistic curve. The fiber orientation was found affected by the placing method and formwork. The ultrasonic wave technique revealed the rebar position along the scan lines with negligible influence of steel fibers.

### **INTRODUCTION**

Ultra-high-performance concrete (UHPC) with a compressive strength of over 150 MPa and significantly fine microstructure is a promising material for a nuclear reactor building's exterior walls considering its very high compressive strength and blast resistance. The research on the casting and mechanical performance of UHPC has been mainly conducted in laboratories with small-scale specimens. To the best of our knowledge, few referred to the large-scale casting of UHPC (Aghdasi et al. 2016, Azmee and Shafiq 2018, Graybeal 2008). Such knowledge, however, is essential for a better understanding of the more realistic behavior of UHPC members and promoting the application of UHPC in construction.

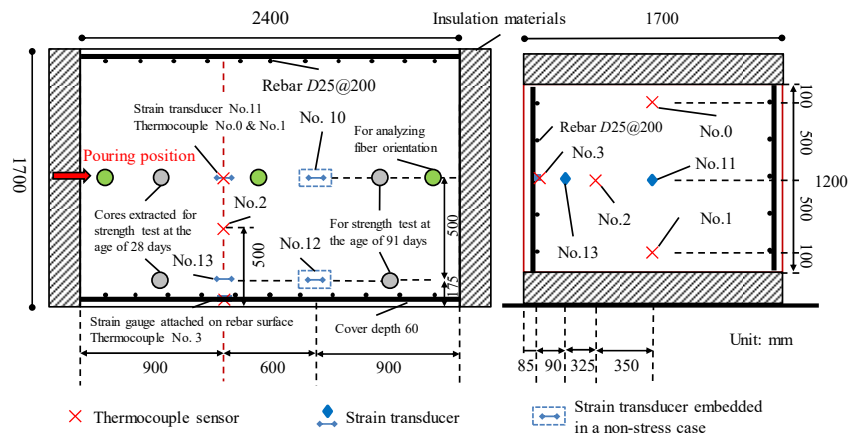
This study aims to verify the large-scale cast-in-place ability of a designed UHPC mixture that includes a hybrid of steel and polypropylenes fibers and coarse aggregates. It focused on on-site casting following Japan's existing building standards, JASS 5 (AIJ 2009) and JASS 5N (AIJ 2013), without special heat, pressure, or moisture curing. Several issues related to mass concrete construction were considered herein, including working time, thermal and autogenous deformation, curing temperature-dependent strength development, fiber orientation influenced by placing method, and rebar probe for installing post

anchors. This study was carried out within the project of “Development of technical infrastructure for upgrading materials, structures and construction methods of nuclear power plant buildings”.

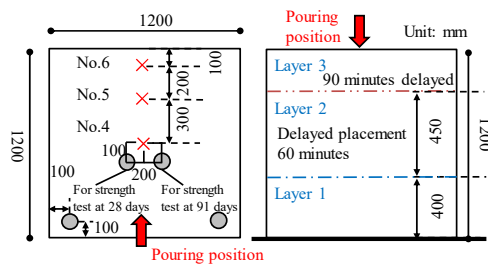
## EXPERIMENTAL PROGRAM

### Specimen Geometry

Concrete members of a nuclear reactor building typically have a large cross-section that requires a considerable volume for a single casting. Therefore, this study used a wall specimen of 2400×1700×1200 mm<sup>3</sup> named specimen A to verify the designed concrete mixture’s on-site large-casting capability (see Figure 1). The steel reinforcing bars with a nominal diameter of 25 mm were embedded at an interval of 200 mm, and the concrete cover depth was 60 mm. The specimen was thermally insulated with polystyrene foam of 150mm thick except the thickness direction. On the other hand, to examine the effect of delayed placement on casting consistency, a cubic specimen of 1200 mm named specimen B was cast layer by layer.



(a) Specimen A



(b) Specimen B

Figure 1. Specimen geometry.

### Concrete Mixture Compositions

Table 1 shows the properties of the materials used for UHPC, and Table 2 shows the mixture proportion. Such a mixture composition was decided in a preliminary study (Nishioka et al. 2018), which investigated the effects of steel fiber geometry and fiber dosage on the workability and flexural performance of UHPC. The cement was commercial silica fume cement produced by pre-mixing low heat Portland cement and ultra-fine silica fume in a mass fraction of 0.9 and 0.1. The spherical micro silica flour with an average diameter of 0.4 μm was added to enhance the flowability. The blending steel fibers of short straight and

long hook-ended were added in a total volume fraction of 1.0% to ensure proper workability for large-scale casting. Furthermore, the preliminary study showed that its mechanical performance was comparable to that reinforced with 1.0% long hooked end fibers. The bulk volume of coarse aggregates was lowered to  $0.3 \text{ m}^3/\text{m}^3$  to accommodate the long steel fibers.

Table 1: Properties of UHPC materials.

Materials	Notations	Properties / Specific gravity [ $\text{g}/\text{cm}^3$ ]
Cement	SFC	Blaine fineness of $6160 \text{ cm}^2/\text{g}$ / 3.08
Micro silica flour	MSF	A by-product of electro fused zirconia with 95.2% $\text{SiO}_2$ and BET surface area of $6.9 \text{ m}^2/\text{g}$ / 2.20
Sand	S	Crushed sandstone / 2.63 (saturated-surface-dry)
Coarse aggregate	G	Sandstone <15mm / 2.65 (saturated-surface-dry)
High-range water-reducing agent	HRWRA	Polycarboxylate type / 1.05 ~ 1.13
Steel fiber	H	30 mm long with an aspect ratio of 80 / 7.85
	SS	13mm long with an aspect ratio of 65 / 7.85
Polypropylene fiber	PP	2mm long / 0.93

Table 2: Mixture proportions of UHPC.

W/B	s/a	Water	Binder		Aggregates		HRWRA	Fiber		
			SFC	MSF	S	G		H	SS	PP
(%)			(kg/m <sup>3</sup> )				(%. b)	(vol. %)		
16.0	64.0	155	947	22	855	485	2.8	0.5	0.5	0.11

### **Mixing And Casting**

The UHPC was produced at a ready-mix plant with a double-axis forced mixer. The dry components were mixed for 30 seconds, and then water pre-mixed with HRWRA was added and mixed for two minutes. The coarse aggregates were added afterward, and the mixing continued for another two minutes. After that, the fibers were slowly included to ensure uniform dispersion, and the mixture was further mixed for three minutes before discharge.

The ready UHPC was transported by agitators to the testing site and poured into the formworks following different casting plans. For specimen A, the UHPC was placed in a continuous manner, as shown in Figure 1. In contrast, specimen B was cast in three layers, in which a delay of 60 minutes between the first two layers and a further delay of 90 minutes for layer three were purposely made. Given the high viscosity of the UHPC, the casting applied internal vibration to achieve satisfactory compaction, which was performed at prespecified locations with an interval of 60 cm following JASS 5 (AIJ 2009) and JASS 5N (AIJ 2013) for 15 seconds. The two specimens were demolded at the age of seven days.

### **Testing Methods**

For testing the fresh properties of the UHPC, slump flow and air content were measured following JIS A 1150 (JSA 2007) and JIS A 1128 (JSA 2019), and the L-type flow test was conducted according to JSCE-

F514 (JSCE 2010). The data at the time of loading, at the time of discharge, 60 minutes, 90 minutes, and 120 minutes after the loading were compared to check the working time of the UHPC mixture.

The temperature rise due to the heat of hydration was investigated using the thermocouple sensors and those built in the strain transducers, which were placed at various locations, as shown in Figure 1. For studying autogenous strain, non-stress cases with embedded strain transducers were installed 175mm from the surface and at the center, respectively. It should be noted that the strains measured with non-stress cases consist of both thermal and autogenous strains. Besides, the rebar strain was monitored with a strain gauge attached to the rebar surface. All the data were recorded since the casting was completed, and the measuring interval was set to ten minutes for long-term testing.

The compressive strength at 28 and 91 days was measured using the cores extracted from both test specimens, as shown in Figure 1. For comparison, the cylindrical specimens of 100 mm in diameter and 200 mm high were also prepared during the casting. This study employed two curing procedures: standard curing in water and on-site curing in sealed conditions.

For studying the effect of placement on fiber orientation, the core specimens of 100 mm high at various positions, as shown in Figure 2, were extracted and scanned using X-ray computed tomography (CT). A high voltage of 220 kV and a current of 140  $\mu$ A were applied to obtain a good X-ray penetration through the dense UHPC. A 0.5 mm thick copper filter was employed between the specimen and the X-ray source to avoid artifacts such as beam hardening. The obtained 3D CT images with a voxel size of 0.13 mm were processed using VG Studio MAX for analyzing fiber orientation. A global gray-value threshold, which was the average of the mean gray-values of a selected fiber area and a UHPC matrix area, was used to identify steel fibers. Then, an opening-closing procedure was carried out to refine the fiber areas, resulting in a reasonable fiber volume estimate. The details of the employed method and its applicability can be found in Qiao et al. (2021). This study analyzed each fiber voxel's orientation without separating individual fibers, as it is challenging for the mixture of two types of fibers.

Since installing post-anchors requires the knowledge of the location of rebar and concrete voids, the applicability of the ultrasonic wave reflection technique for the rebar probe was examined in this study. An ultrasonic multi-channel tomography instrument utilizing transverse waves was adopted, which allowed for visualization of internal conditions of concrete. For measuring concrete cover depth, the velocity of transverse waves through the UHPC was decided as 3093 m/s using a prismatic specimen of 530 $\times$ 150 $\times$ 150 mm<sup>3</sup>, which was fabricated with the same UHPC mixture. The test scanned three longitudinal lines to find the vertical rebars embedded in specimen A.

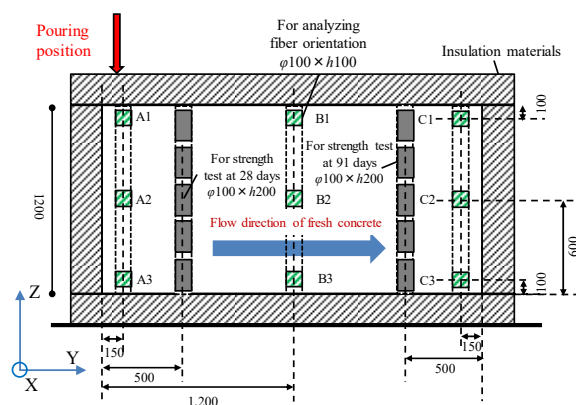


Figure 2. Positions of core extractions for CT scan.

## EXPERIMENTAL RESULTS AND DISCUSSION

### Workability

Figure 3 presents the fresh properties of the UHPC mixture. The slump flow varied insignificantly within two hours after the time of loading. Similarly, the air content remained in the targeted range of  $2.0 \pm 1.0\%$ , confirming the working time of two hours. Regarding the L-type flow test, the flow speed appears to increase until the discharge time, suggesting that extra mixing time may be needed for full activation of HRWRA. After that, the flow speed decreased with time, showing a gradual increase in viscosity. However, following the existing construction standard, proper internal vibration led to satisfactory filling status. As shown in Photo 1, the core sample extracted from specimen B shows good conditions without visible cold joints or large voids.

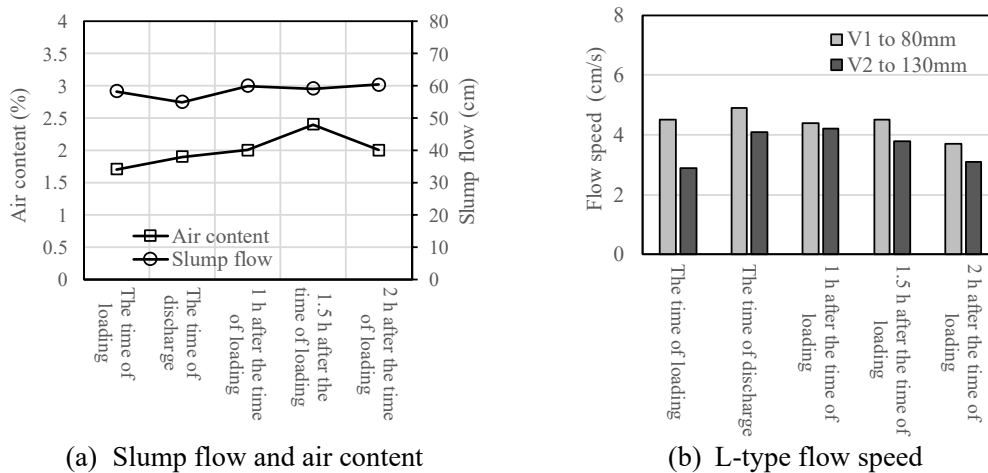


Figure 3. Test results of fresh properties.

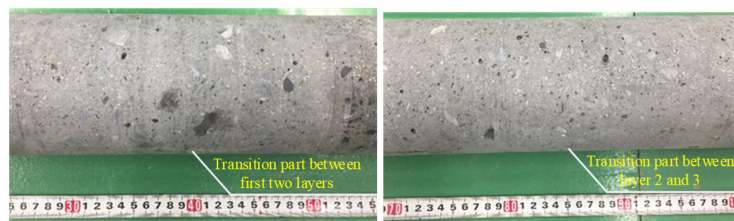


Photo 1. Surface conditions of concrete cores extracted from the center of Specimen B.

### Temperature History and Strain Development

Figure 4 shows the temperature histories within specimens A and B, respectively. For specimen A, the center reached  $78\text{ }^{\circ}\text{C}$  at 2.5 days, which was about  $20\text{ }^{\circ}\text{C}$  higher than that of the surface layer. The temperature variation reached equilibrium with the ambient environment at about 28 days. In comparison, the center of specimen B had a lower maximum temperature of  $59\text{ }^{\circ}\text{C}$  resulting from the smaller specimen size and lack of thermal insulation. Although significant temperature gradients between the specimen center and the surface were observed, no thermal-induced cracks could be found on the cores extracted from both specimens.

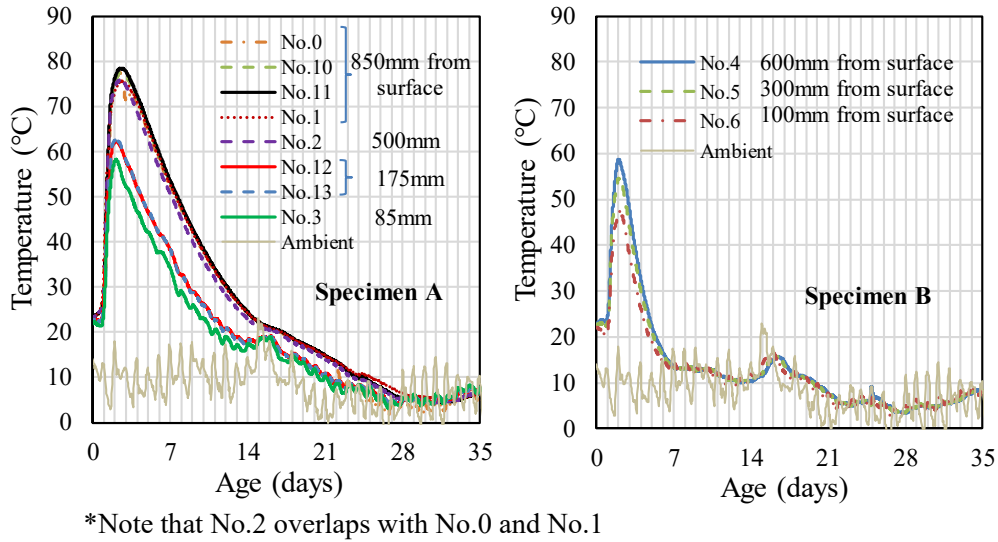


Figure 4. Temperature history.

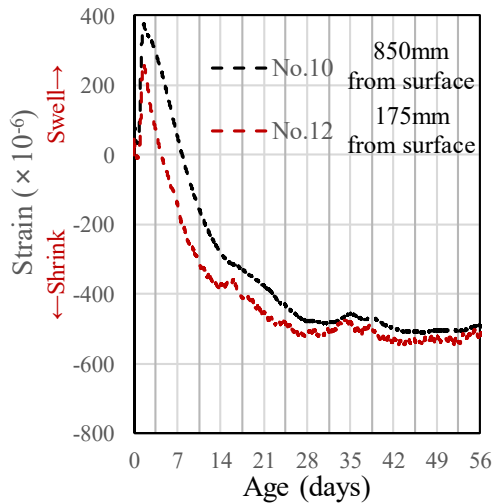


Figure 5. Concrete strains measured with non-stress cases

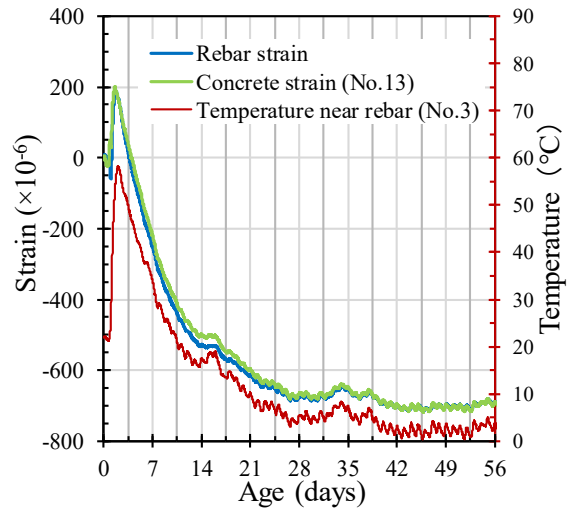


Figure 6. The development of rebar strain

Figure 5 shows the strains measured using the strain transducers embedded in the non-stress cases. The center yielded more expansive strains due to the higher temperature rise, while its strain decreased to a similar value to that of the surface layer during the cooling. The autogenous strain was decided by subtracting the measured strain with the thermal strain using an assumed coefficient of thermal expansion (CTE). The CTE of concrete varies with time at an early age (Bjøntegaard and Sellevold 2001), which is difficult to measure. Therefore, this study assumed the CTE of the early UHPC as  $11.0 \mu/\text{°C}$ , according to NF P 18-710 (AFNOR 2016). The final asymptotic value of autogenous shrinkage was estimated as  $280 \mu$  for both the specimen center and the surface layer. It was notably smaller than typical values of high-performance concrete ( $600 \sim 700 \mu$  as specified in AIJ recommendation 2013). It can be ascribed to the effect of shrinkage-reducing admixture in HRWRA (Yoo et al. 2015). Meanwhile, three prismatic specimens of  $400 \times 100 \times 100 \text{ mm}^3$  cast with the same UHPC were prepared for studying autogenous

shrinkage. They were cured in sealed conditions at 20 °C. The average autogenous shrinkage of 240 μ was decided at 220 days.

Figure 6 compares the rebar strain with the concrete strain measured nearby. It should be noted that the concrete strain measured without the non-stress case (No. 13) included the restraint effect of surrounding concrete. Hence, it is smaller than No.12, although they were subjected to similar temperature histories, as shown in Figure 4. As shown in Figure 6, the rebar and the neighboring concrete strains agreed due to a low reinforcement ratio.

### Strength Development

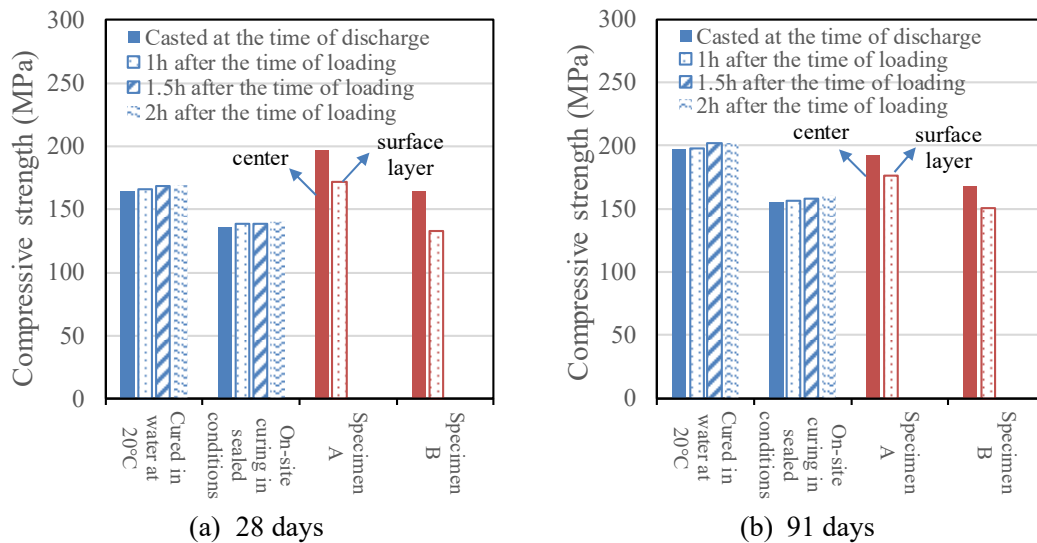


Figure 7. Comparison of compressive strengths under different curing conditions.

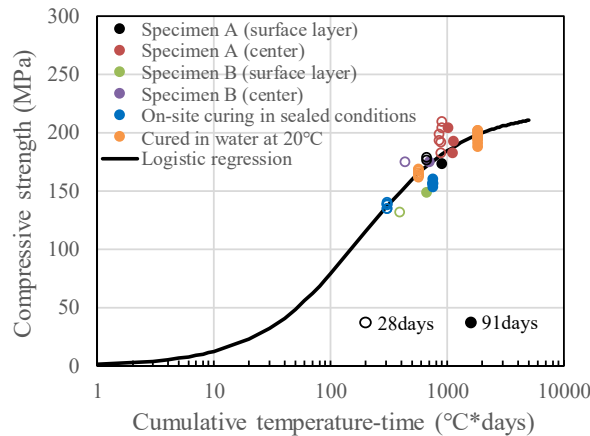


Figure 8. Relation of compressive strengths with cumulative temperature-time.

Figure 7 compares the compressive strengths of the cylindrical specimens prepared with different conditions with those of the core samples extracted from specimens A and B. All cylindrical specimens showed satisfied compressive strengths with the negligible effect of delayed placement. Even those cured on-site at a low temperature ranging from 0 to 10 °C reached the specified compressive strength of 150

MPa at 91 days. As for the core samples, the center of specimen A showed the highest strength at 28 days, but the strength gain was insignificant after that. It is clear that the elevated temperature history due to hydration heat accelerated concrete strength development.

Figure 8 shows the relation of cumulative temperature-time with compressive strength, which correlated well with a logistic curve following Equation.1 (Taniguchi et al. 2009). The regression results showed that it could take 400 °C\*days to reach the specified compressive strength of 150 MPa.

$$F_c = F_\infty / (1 + \exp(-a(\log_{10}M - b))) \quad (1)$$

Where  $F_\infty$  is the final strength,  $M$  is the cumulative temperature-time, and  $a$  and  $b$  are parameters.

### Fiber Orientation

As shown in Figure 2, a coordinate system was defined for clarifying fiber orientation. The deviation angle against the vertical direction ( $Z$ -axis) and the angle projected on the horizontal plane ( $XY$ -plane) were decided. Figure 9 shows color-coded fiber distributions for the cores along the centerline (see Figure 2), which shows the deviation angle. It appears that the fiber orientation varied greatly because of the continuous pouring from a single location.

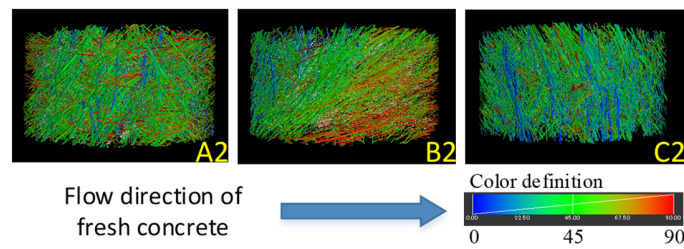


Figure 9. Color-coded fiber distribution by deviation angle.

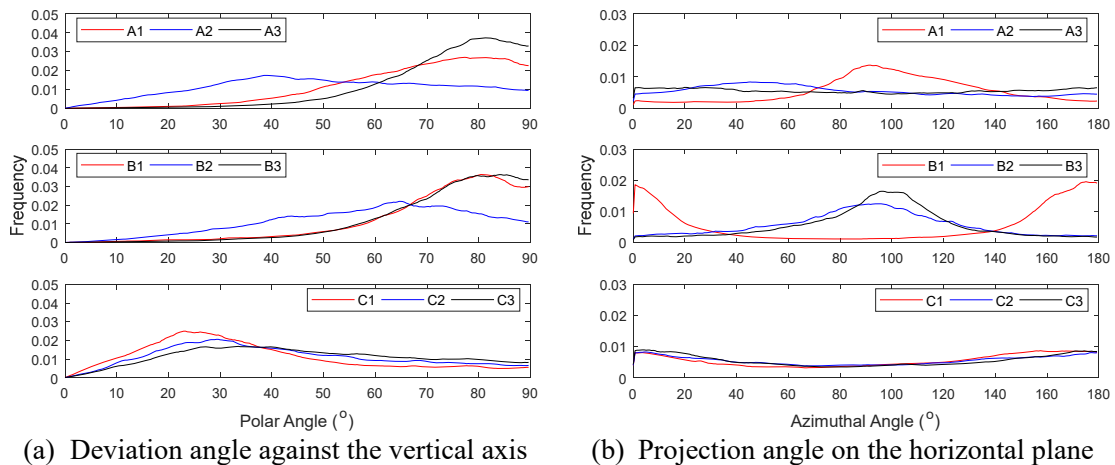


Figure 10. Histograms of orientation angles.

Figure 10 shows the histograms of the deviation angle and the projection angle, respectively. Comparing the midstream labeled as B with the upstream as A, B2 showed a peak shift of the deviation

angle to 60 ~ 70 degrees, and in B1 and B3, the frequency for large angles increased. On the other hand, the peak of the fibers' deviation angle at the downstream labeled as C changed to 20 ~ 30 degrees. These variations indicate that the fibers tended to incline to the horizontal plane parallel to the flow direction as the fresh concrete flowed. In contrast, the fibers hit the formwork downstream and thus faced vertically. As for the projection angle, both upstream and downstream showed randomness, while most fibers aligned with the flow direction at midstream. These results suggest that pouring the fresh UHPC at different locations is preferred to ensure a random fiber orientation.

### Rebar Probe

Figure 11 shows the rebar locations found by ultrasonic waves. The number of vertical rebars and their location along the scan lines agree well with the actual rebar arrangement. The influence of added steel fibers seems negligible. The test, however, overestimated the cover depth due to a larger input of the velocity of the transverse wave. More study is needed for the correct determination of such parameters.

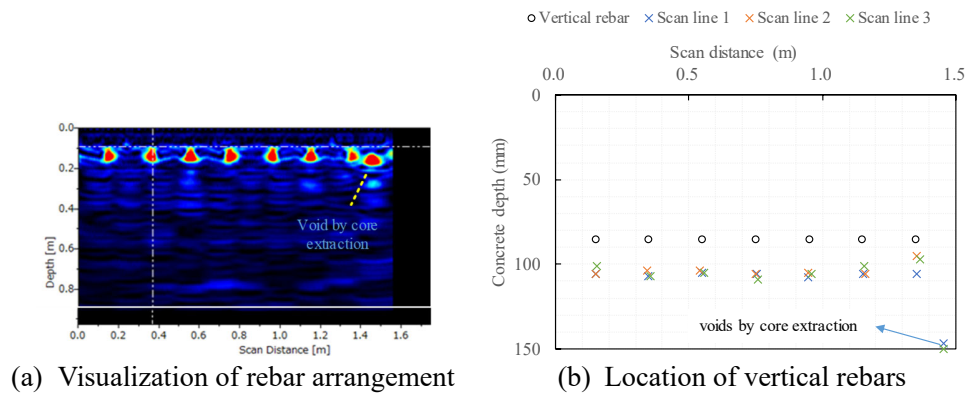


Figure 11. Test results of rebar probe by ultrasonic waves.

## CONCLUSION

This study investigated the large-scale cast-in-place ability of the designed UHPC mixture with a specific compressive strength of 150 MPa. In summary, the following conclusions can be drawn from this study:

1. The designed UHPC mixture is applicable for the cast-in-place practice of large-section members. Utilizing internal vibration following the existing building standards (JASS5 and JASS5N) resulted in satisfactory compaction.
2. Within two hours after loading, the fresh properties and the strength development remained consistent, confirming the working time of two hours. No cold joints formed even with delayed placement up to 90 minutes.
3. The autogenous shrinkage of the UHPC showed a satisfactorily low level of 280  $\mu$ .
4. The flow of fresh concrete impacted strongly on fiber orientation. The casting plan needs to account for the effects of formwork and pouring locations on the concrete flow.
5. The applicability of the ultrasonic wave reflection technique on the probe of rebars embedded in the UHPC was confirmed. However, for concrete cover depth, more study is required to correctly decide the ultrasonic wave's velocity through the UHPC.

This study is part of a research project studying material properties, structural performance, and construction methods of emerging new concrete, aiming for application to nuclear reactor buildings. The cast-in-place ability of heavyweight concrete with a density of 3.5 g/cm<sup>3</sup> and a specified compressive strength of 45 MPa was also examined with similar test procedures, as presented in this paper. The test results confirmed that the designed heavyweight concrete also has the same applicability as conventional concrete following the existing building standards.

## ACKNOWLEDGEMENT

This study was carried out within the project on development of technical basis for improving nuclear safety funded by the Ministry of Economy, Trade and Industry (METI) of Japan.

## REFERENCES

- Aghdasi, P., Heid, A. E. and Chao, S. H., (2016). “Developing ultra-high-performance fiber-reinforced concrete for large-scale structural applications,” *ACI Materials Journal*, 113(5), 559-570.
- Architectural Institute of Japan (AIJ), (2009). *Japanese architectural standard specification for reinforced concrete work (JASS5)*. Tokyo, Japan.
- Architectural Institute of Japan (AIJ), (2013). *Japanese architectural standard specification for reinforced concrete work at nuclear power plants (JASS5N)*. Tokyo, Japan. [in Japanese]
- Architectural Institute of Japan (AIJ), (2013). *Recommendation for practice of high-strength concrete*, Tokyo: AIJ. [in Japanese]
- Azme, N. M. and Shafiq, N., (2018). “Ultra-high-performance concrete: from fundamental to applications,” *Case Studies in Construction Materials*, 9, e00197.
- Bjøntegaard, Ø. and Sellevold, E. J., (2001). “Interaction between thermal dilation and autogenous deformation in high performance concrete,” *Materials and Structures*, 34(5), 266-272.
- Graybeal, B., (2008). “Flexural behavior of an ultra-high-performance concrete I-girder,” *Journal of Bridge Engineering*, ASCE, 13(6), 602-610.
- Japanese Standard Association, (2007). *JIS A 1150 Method of test for slump flow of concrete*. Tokyo, Japan.
- Japanese Standard Association, (2019). *JIS A 1128 Method of test for air content of fresh concrete by pressure method*. Tokyo, Japan.
- Japan Society of Civil Engineers (JSCE), (2010). *JSCE F-514 Test method for L-type flow of self-compacting concrete*. Tokyo, Japan.
- AFNOR, (2016). *NF P 18-710 National addition to Eurocode 2 – design of concrete structures: specified rules for ultra-high-performance fiber-reinforced concrete (UHPFRC)*. Saint-Denis, France.
- Nishioka, Y., Honma, D. and Kojima, M., (2018). “Effects of fiber geometry and dosage on fresh properties and flexural performance of high-strength fiber-reinforced concrete,” *Proceedings of the JCI*, 40(1), 297-302. [in Japanese]
- Qiao, D., Honma, D. and Kojima, M., (2021). “Size effects on flexural behaviour and fibre orientation of ultra-high-performance fibre-reinforced concrete,” *Proceedings of the fib symposium 2021*, Lisbon, Portugal, 449-458.
- Taniguchi, M., Katsura, O., Hama, Y. and Yoshino, T., (2009). “A proposal of compressive strength prediction method enhanced the applicable range of water-cement ratio,” *Journal of Structural and Construction Engineering (Transactions of AIJ)*, 74(641), 1205-1210. [in Japanese]
- Yoo, D. Y., Banthia, N. and Yoon, Y. S., (2015). “Effectiveness of shrinkage-reducing admixture in reducing autogenous shrinkage stress of ultra-high-performance fiber-reinforced concrete,” *Cement and Concrete Composites*, 64, 27-36.